Time-resolved X-ray scattering by electronic wave packets: analytic solutions to the hydrogen atom

Simmermacher, Mats; Henriksen, Niels Engholm; Møller, Klaus Braagaard

Published in:
Physical Chemistry Chemical Physics

Link to article, DOI:
10.1039/c7cp01831b

Publication date:
2017

Document Version
Peer reviewed version

Journal Name

ARTICLE TYPE

Cite this: DOI: 10.1039/xxxxxxxxxx

Time-Resolved X-Ray Scattering by Electronic Wave Packets: Analytic Solutions to the Hydrogen Atom†

Mats Simmermacher, Niels E. Henriksen,* and Klaus B. Møller

Received Date
Accepted Date

DOI: 10.1039/xxxxxxxxxx

www.rsc.org/journalname

Modern pulsed X-ray sources permit time-dependent measurements of dynamical changes in atoms and molecules via non-resonant scattering. The planning, analysis, and interpretation of such experiments, however, require a firm and elaborated theoretical framework. This paper provides a detailed description of time-resolved X-ray scattering by non-stationary electronic wave packets in atomic systems. A consistent application of the Waller-Hartree approximation is discussed and different contributions to the total differential scattering signal are identified and interpreted. Moreover, it is demonstrated how the scattering signal of wave packets in the hydrogen atom can be expressed analytically. This permits simulations without numerical integration and establishes a benchmark for both efficiency and accuracy. Based on that, scattering patterns of an exemplary wave packet in the hydrogen atom are computed for different points in time. In doing so, distinct features of time-resolved X-ray scattering by non-stationary electronic wave packets are illustrated and accentuated in greater detail than it has been done before.

1 Introduction

Recent advances in the generation of coherent, intense, and ultrashort X-ray pulses provide novel and promising opportunities for imaging rapid dynamics in atoms and molecules via non-resonant time-resolved scattering. Current X-ray Free-Electron Laser facilities permit measurements with temporal resolutions of the order of tenths of femtoseconds [1–4] and allow to track nuclear motions and structural changes in chemical reactions in real time [5–12]. The durations of these pulses may be further decreased to attoseconds in the future [13–17]. It can thus be assumed that temporal changes in the X-ray scattering signal due to even faster electronic motions will be detectable.

The interpretation of such changes, however, is significantly complicated by the quantum mechanical nature of the motion of bound electrons, the non-classical character of the light-matter interaction, and the lack of intensification of coherent scattering as in Bragg diffraction by crystalline matter. It has already been pointed out that the scattering signal of non-stationary electronic wave packets in atoms and molecules does not reveal their instantaneous electron densities [18]. The semi-classical approach successfully applied in static X-ray scattering, *i.e.* the assignment of the signal to the Fourier transform of those densities, was proven inadequate. Instead, the scattering event has to be described by quantum electrodynamics, taking into account that photons are quantized excitations of electromagnetic field modes [19].

In order to exploit the potential of X-ray scattering experiments with femto- or attosecond resolution, a firm and elaborate theoretical framework for their planning, analysis, and interpretation is necessary. This has been pioneered in the nineties [20–22] and was addressed in several recent publications [18,23–30]. Nevertheless, some aspects of the theory remain opaque. Though the equations provided in the references are compact and generally applicable, the immediate insights they provide are relatively limited. A deeper understanding of the characteristics of time-resolved X-ray scattering requires a more detailed and more specific analysis.

In section 2 of this paper, the scattering signal of non-stationary electronic wave packets in atoms is rigorously described. Static and time-dependent contributions are identified and related to their constituting scattering matrix elements. In section 3, a physical interpretation of these elements is provided. Section 4 summarizes the derivation of an approach to express and evaluate the scattering signal by any wave packet in the hydrogen atom analytically. Finally, the distinctive features of time-resolved X-ray scattering by non-stationary electronic wave packets are illustrated by means of an example in section 5.

Department of Chemistry, Technical University of Denmark, 2800 Lyngby, Denmark. E-mail: neh@kemi.dtu.dk

† Electronic Supplementary Information (ESI) available: Detailed discussion of the consequences of an inconsistent application of the Waller-Hartree approximation, derivation of equations (17) and (18), tables for expansions of all real-valued atomic orbitals with principal quantum numbers $n \in \{1,2,3,4\}$ in the parabolic eigenstate basis, tables for a rotation of all $|\mathbf{d}\rangle$ and $|\mathbf{f}\rangle$ orbitals in three-dimensional space, details of the evaluation of the scattering patterns, and a figure that shows the influence of the probe pulse duration on the intensity of the static inelastic scattering. See DOI: 10.1039/b000000x/

2 General Theory

In time-resolved X-ray scattering experiments, a pulse of electromagnetic radiation prepares a non-stationary wave function $|\Psi(t)\rangle$ by excitation of a material system initially in its ground state. Subsequently, a second pulse of X-rays is scattered. The time lag between these two pulses is referred to as the pump-probe delay. The evolution of $|\Psi(t)\rangle$ describes the dynamics of the system that are to be probed at different pump-probe delays. In the following, the wave function is assumed to be a non-stationary electronic wave packet:

$$|\Psi(t)\rangle = \sum_i^N c_i \, e^{-\imath E_i t/\hbar} \cdot |\psi_i\rangle. \tag{1}$$

The basis vectors $|\psi_i\rangle$ are eigenstates of the field-free Hamiltonian of the material system with energy E_i, the multipliers c_i are expansion coefficients, $\imath$ denotes the imaginary unit, and $\hbar$ is the reduced Planck constant.

The interaction of hard X-ray photons and $|\Psi(t)\rangle$ can be described by use of first-order perturbation theory and a quantized electromagnetic X-ray field [18,24–26]. For equation (1), the time-resolved differential scattering signal per solid angle, $dS/d\Omega$, is given as [25]:

$$\begin{aligned}\frac{dS}{d\Omega} = \frac{d\sigma_\mathrm{t}}{d\Omega} \cdot \int_{-\infty}^{+\infty} I(t) \sum_{i,j} \sum_f^\infty c_i \, c_j^* \, e^{-\imath \omega_{ij} t} \\ \times \int L_{fi} \, L_{fj}^* \, \frac{\omega_\mathrm{s}}{\omega_0} \, F\left(\omega_\mathrm{s} + \omega_{fij}\right) \, d\omega_\mathrm{s} \, dt.\end{aligned} \tag{2}$$

Equation (2) involves the differential Thomson cross-section $d\sigma_\mathrm{t}/d\Omega$, a directional measure of elastic scattering of electromagnetic radiation by free electrons. It contains the intensity time profile $I(t)$ as well as the power spectral density $F\left(\omega_\mathrm{s} + \omega_{fij}\right)$ of the X-ray probe pulse. Moreover, ω_0 and ω_s are the angular frequencies of the incident and scattered photons, whereas $\omega_{ij} = (E_i - E_j)/\hbar$ and $\omega_{fij} = \left(E_f - \left[E_i + E_j\right]/2\right)/\hbar$ refer to differences in energies of their corresponding electronic states. Finally, the expression contains scattering matrix elements:

$$L_{fi} = \langle \psi_f | \hat{\boldsymbol{L}} | \psi_i \rangle. \tag{3}$$

Here, the scattering operator $\hat{\boldsymbol{L}} = \sum_n e^{\imath \boldsymbol{q} \boldsymbol{r}_n}$ connects the two eigenstates $|\psi_i\rangle$ and $|\psi_f\rangle$. The scattering vector $\boldsymbol{q} = \boldsymbol{k}_0 - \boldsymbol{k}_\mathrm{s}$ in the exponent of the operator refers to the vector difference of the wave vectors of the incident and the scattered photons, respectively. The sum runs over all electrons of the system and $\boldsymbol{r}_n$ is the spatial coordinate of the electron with index n. These coordinates are the variables of integration in equation (3).

Due to the ω_s-dependence of the $\boldsymbol{q}$-vector, the two scattering matrix elements in equation (2) are involved in the integral over the frequency. If $\omega_\mathrm{s} \approx \omega_0$, however, $\boldsymbol{q}$ and thus $L_{fi} \, L_{fj}^*$ become independent of ω_s. This assumption was first used by Waller and Hartree [31] and is sometimes termed the "elastic approximation". Despite its name, it does not imply that the scattering becomes purely elastic. It is only assumed that the transfer of energy between the photon and the material system is small compared to the mean photon energy of the probe pulse and that its effect on $\boldsymbol{q}$ is negligible. This is well justified as long as the transition energies of the material system are orders of magnitude lower than the mean energies of the incident photons. Since the relevant electronic eigenstates of atoms and molecules are typically separated by not more than a few electron volts, this condition is usually satisfied in time-resolved X-ray scattering with photon energies of several keV. Hence, equation (2) becomes:

$$\frac{dS}{d\Omega} \approx \frac{d\sigma_\mathrm{t}}{d\Omega} \cdot \int_{-\infty}^{+\infty} I(t) \sum_{i,j} \sum_f^\infty c_i \, c_j^* \, e^{-\imath \omega_{ij} t} \, \tilde{L}_{fi} \, \tilde{L}_{fj}^* \, W_{fij}(\Delta\omega) \, dt. \tag{4}$$

The tilde on top of $\tilde{L}_{fi} \, \tilde{L}_{fj}^*$ labels the scattering matrix elements to be independent of ω_s. The remaining integral over ω_s is written as the function $W_{fij}(\Delta\omega)$:

$$W_{fij}(\Delta\omega) = \int_{\omega_0 - \Delta\omega}^{\omega_0 + \Delta\omega} F\left(\omega_\mathrm{s} + \omega_{fij}\right) \, d\omega_\mathrm{s}. \tag{5}$$

The lower and upper limits of the integral are defined by a detection window of $\pm\Delta\omega$ around the mean angular frequency ω_0. It is important to note that $\Delta\omega$ has to be small in comparison with ω_0 in order to be consistent with the approximation introduced above. In a previous derivation [25], it was assumed that the integral runs from zero to infinity, meaning that all photons are detected regardless of their energies. This resulted in an expression for time-dependent incoherent scattering published already in 1998 [22], but violates, strictly speaking, the condition under which equation (4) is justified. Consequently, the information contained in scattering by single electrons is lost, as discussed in the Supplementary Information[†]. It is therefore necessary to restrict the range of detection to scattered photons with frequencies in the vicinity of ω_0.

The function $W_{fij}(\Delta\omega)$ imposes a weight on the terms of the sum over f in equation (4). It accounts for the number of incident X-ray photons with frequencies that can be shifted by ω_{fij} to frequencies ω_s within the detection range of $\pm\Delta\omega$ around ω_0. The shift ω_{fij} corresponds to an inelastic energy transfer between the photon and the wave packet. Since the value of $W_{fij}(\Delta\omega)$ decreases with an increase in ω_{fij}, the function effectively introduces an upper limit into the sum over f.

Equation (4) is similar to the expression used in the seminal contribution by Dixit *et al.* [18]. There are, however, some differences: First, equation (4) is not based on the assumption that the dynamics of the wave packet is frozen during the scattering process. The convolution with $I(t)$ is explicitly taken into account. Second, the limits of integration in equation (5) have been introduced as a direct consequence of the approximation $\omega_\mathrm{s} \approx \omega_0$. Third, equation (4) is written in terms of scattering matrix elements and not as one compact expectation value of density operators. This permits further simplifications and facilitates the identification, physical interpretation, and evaluation of separable contributions.

To begin with, equation (4) contains terms diagonal and off-diagonal in i and j that can be partitioned:

$$\frac{dS}{d\Omega} \propto \sum_{i}^{N} I \cdot D_i + 2 \cdot \sum_{i}^{N-1} \sum_{j>i}^{N} \int_{-\infty}^{+\infty} I(t)\, Z_{ij}(t)\, dt. \tag{6}$$

The sum of the diagonal elements D_i in equation (6) defines the static average of the differential scattering signal, whereas the sum of the integrated, off-diagonal elements Z_{ij} describes its time-dependent modulation. The elements are given as:

$$D_i = |c_i|^2 \cdot \sum_{f}^{\infty} |\tilde{L}_{fi}|^2\, W_{fii}(\Delta\omega), \tag{7}$$

$$Z_{ij}(t) = \mathrm{Re}\Big[c_i\, c_j^*\, e^{-\imath\omega_{ij}t} \cdot \sum_{f}^{\infty} \tilde{L}_{fi}\, \tilde{L}_{fj}^*\, W_{fij}(\Delta\omega)\Big]. \tag{8}$$

Due to the real part in equation (8), $Z_{ij}(t)$ is invariant under interchange of its sub- and superscript. Hence, the $N \times N$ sized matrix of all elements is symmetric. This permits the reduction of the double sum in equation (6) to $j > i$ and results in the factor of 2. Since D_i contains no time variable, only $Z_{ij}(t)$ is convoluted with the intensity time profile $I(t)$ and D_i is simply multiplied by the total integrated intensity $I = \int_{-\infty}^{+\infty} I(t)\, dt$. According to Euler's formula, equation (8) can be written in terms of real-valued trigonometric functions:

$$Z_{ij}(t) = \cos(\omega_{ij}t)\, \mathrm{Re}\big[O_{ij}\big] + \sin(\omega_{ij}t)\, \mathrm{Im}\big[O_{ij}\big]. \tag{9}$$

The element O_{ij} in equation (9) is a product of two different scattering matrix elements, their expansion coefficients, and their weights from equation (5):

$$O_{ij} = c_i\, c_j^* \cdot \sum_{f}^{\infty} \tilde{L}_{fi}\, \tilde{L}_{fj}^*\, W_{fij}(\Delta\omega). \tag{10}$$

In the following, the intensity time profile $I(t)$ will be described by a normalized Gaussian function:

$$I(t) = \frac{1}{\sigma\sqrt{2\pi}}\, e^{-\frac{(t-\tau)^2}{2\sigma^2}}. \tag{11}$$

The pulse given in equation (11) is centered at the pump-probe delay τ and has a duration defined as the full width at half maximum (FWHM) of $d_\mathrm{p} = 2\sqrt{2\ln 2}\,\sigma$. With equations (9) and (11), the integral over time in equation (6) can be solved analytically:

$$\int_{-\infty}^{+\infty} I(t)\, Z_{ij}(t)\, dt = e^{-\frac{1}{2}(\omega_{ij}\sigma)^2} \cdot \Big(\cos(\omega_{ij}\tau)\, \mathrm{Re}\big[O_{ij}\big] + \sin(\omega_{ij}\tau)\, \mathrm{Im}\big[O_{ij}\big]\Big). \tag{12}$$

The two trigonometric functions $\cos(\omega_{ij}\tau)$ and $\sin(\omega_{ij}\tau)$ in equation (12) determine the magnitude by which the real and imaginary parts of the element O_{ij} contribute to the scattering signal at a given pump-probe delay τ. The exponential factor $\exp(-\frac{1}{2}(\omega_{ij}\sigma)^2)$ accounts for the effect of the finite duration of the probe pulse. It is always smaller than one and decreases rapidly with an increasing ratio of the pulse duration to the period of the oscillation, d_p/T_{ij}, where $T_{ij} = 2\pi/\omega_{ij}$. Hence, the exponential factor determines to what extent the time-dependent modulation of the scattering signal can be temporally resolved.

Assuming coherence of the probe pulse, the power spectral density $F(\omega_\mathrm{s} + \omega_{fij})$ has the following Gaussian shape with the same σ as defined for $I(t)$:

$$F(\omega_\mathrm{s} + \omega_{fij}) = \sqrt{\frac{2}{\pi}}\, \sigma\, e^{-2\sigma^2(\omega_\mathrm{s} - \omega_0 + \omega_{fij})^2}. \tag{13}$$

With equation (13), the weights in equation (5) are:

$$W_{fij}(\Delta\omega) = \frac{1}{2} \cdot \Big[\mathrm{erf}\Big(\sqrt{2}\sigma(\omega_{fij} + \Delta\omega)\Big) - \mathrm{erf}\Big(\sqrt{2}\sigma(\omega_{fij} - \Delta\omega)\Big)\Big]. \tag{14}$$

Equation (14) contains two error functions. For a given $\Delta\omega$, W_{fij} takes maximum values when f is equal to i or j and converges to a minimum when $f \to \infty$.

Note that in the framework of equations (11) and (13) a shorter pulse duration implies a larger frequency bandwidth, since σ defines the widths of both $I(t)$ and $F(\omega_\mathrm{s} + \omega_{fij})$. Consequently, a decrease in the pulse duration results in a reduction of the number of photons with angular frequencies inside of $\omega_0 \pm \Delta\omega$ and thereby leads to a decrease in the intensity of the detected scattering signal. It is important to emphasize that each term of D_i and O_{ij} in equations (7) and (10), respectively, is affected differently by this decrease in intensity: Every contribution to the scattering signal corresponds to a particular transfer of energy ω_{fij}. If the contribution is elastic, the angular frequency ω_{fij} is zero and equation (14) simplifies to $\mathrm{erf}(\sqrt{2}\sigma\,\Delta\omega)$. This function vanishes as $\sigma \to 0$ and approaches one as $\sigma \to \infty$. If at least two of the indices in equation (14) are different, however, W_{fij} becomes zero for both $\sigma \to 0$ and $\sigma \to \infty$ and displays an optimum in between. The value of σ where this optimum occurs depends on both ω_{fij} and $\Delta\omega$.

Physically, this can be understood as follows: If the frequency bandwidth of the incident probe pulse is smaller than $\omega_0 \pm \Delta\omega$, almost all elastically scattered photons are detected. If the bandwidth is increased, less photons fall into the range of detection and the signal becomes weaker. For inelastically scattered photons, the situation is different. Only photons with incident angular frequencies that fall into $\omega_0 \pm \Delta\omega$ after a shift by ω_{fij} are detected. If both $\Delta\omega$ and the frequency bandwidth are small in comparison to ω_{fij}, most photons are scattered to energies outside of the range of detection and the signal is weak.

A loss of time-dependent modulation of the scattering signal at very short probe pulse durations was reported by Dixit *et al.* [18]. In the present context, such a loss is ascribed to the coherence of the probe pulse and a finite width of the detection window: For a

given $\Delta\omega$, the weights W_{fij} in equations (7) and (10) define a frequency bandwidth (or pulse duration) that permits the detection of the largest proportion of photons that carry time-dependent information. This explanation deviates from the previously published one that related the loss of contrast to the time-scale of the electronic motion [18] and will be further illustrated in section 5.

3 Physical Interpretation

In coherent X-ray diffractometry of stationary systems, the scattering signal can be described by absolute squares of Fourier transforms of the one-electron density. It has therefore been suggested to relate the time-dependent scattering of non-stationary wave packets to absolute squares of Fourier transforms of the time-dependent one-electron density [29]. However, such an approach essentially leads to wrong results, as has been revealed by Dixit *et al.* [18]. In order to understand the fundamental difference of the more involved description given in the previous section, it is illustrative to re-express equations (7) and (10) in terms of expectation values of the one-electron density operator $\rho_{fi}(\boldsymbol{r})$ and their Fourier transforms $\mathscr{F}_{\boldsymbol{r}}\left[\rho_{fi}(\boldsymbol{r})\right](\boldsymbol{q})$ from $\boldsymbol{r}$- into $\boldsymbol{q}$-space:

$$\rho_{fi}(\boldsymbol{r}) = \sum_{n=1}^{N_e} \left\langle \psi_f \middle| \hat{\delta}(\boldsymbol{r}-\boldsymbol{r}_n) \middle| \psi_i \right\rangle, \tag{15}$$

$$\mathscr{F}_{\boldsymbol{r}}\left[\rho_{fi}(\boldsymbol{r})\right](\boldsymbol{q}) = \int_{-\infty}^{\infty} e^{\imath \boldsymbol{q}\boldsymbol{r}}\, \rho_{fi}(\boldsymbol{r})\, d\boldsymbol{r}. \tag{16}$$

As shown in the Supplementary Information†, equations (15) and (16) can be used to obtain the following alternative expressions for D_i and O_{ij}:

$$D_i = \left|c_i\right|^2 \cdot \sum_f^{\infty} \left|\mathscr{F}_{\boldsymbol{r}}\left[\rho_{fi}(\boldsymbol{r})\right](\boldsymbol{q}_0)\right|^2 W_{fii}(\Delta\omega), \tag{17}$$

$$O_{ij} = c_i\, c_j^* \cdot \sum_f^{\infty} \mathscr{F}_{\boldsymbol{r}}\left[\rho_{fi}(\boldsymbol{r})\right](\boldsymbol{q}_0)\, \mathscr{F}_{\boldsymbol{r}}^*\left[\rho_{fj}(\boldsymbol{r})\right](\boldsymbol{q}_0)\, W_{fij}(\Delta\omega). \tag{18}$$

The zero in subscript of $\boldsymbol{q}_0$ in equations (17) and (18) labels the scattering vector to be independent of ω_s.

Equation (17) shows that the element D_i is a weighted sum of absolute squares of Fourier transformed expectation values of the one-electron density operator $\rho_{fi}(\boldsymbol{r})$ associated with the state $\left|\psi_i\right\rangle$. The diagonal term with $f = i$ describes coherent elastic scattering on the one-electron density. The off-diagonal terms with $f \neq i$ allow for inelastic energy transfer from the incident X-ray photon to the material system or *vice versa* by electronic Raman transitions. If the expectation values of the one-electron density operator ρ_{fi} are real—a condition that will be fulfilled when the eigenstates are chosen to be real—the pattern of D_i has to be centrosymmetric in $\boldsymbol{q}$-space, *i.e.* the inversion center has to be an element of its corresponding point group. This requirement is a consequence of the occurrence of the absolute squares of the Fourier transforms in equation (17) and known as Friedel's law [32].

In contrast, the element O_{ij} in equation (18) involved in the time-dependent part of the scattering signal is not related to the absolute square of a single Fourier transform and may therefore give rise to a non-centrosymmetric pattern. It is a weighted sum of products of two different, Fourier transformed expectation values of the one-electron density operator and describes scattering by two eigenstates that are superposed in the wave packet. Thus, the element O_{ij} reveals non-local correlations of the X-ray photon and the evolving material system in the scattering process. Together with the off-diagonal contributions to D_i, it accounts for the quantum mechanical nature of the light-matter interaction [18].

4 Theory of the Hydrogen Atom

In the following, the general considerations of the last section will be applied to electronic wave packets of superposed eigenstates in the hydrogen atom. The matrix elements in D_i and O_{ij} can, in principle, be evaluated directly in a basis of real-valued atomic orbitals. It is possible to expand the scattering operator $\hat{\boldsymbol{L}}$ in terms of spherical Bessel functions and spherical harmonics [18,24] and to evaluate the angular integrals analytically by use of Clebsch-Gordon coefficients [33]. For the remaining radial integrals, however, no analytic solution is known. Hence, it is necessary to evaluate them numerically—a task that is computationally demanding even for the hydrogen atom [18]. As will be demonstrated in this section, one can overcome this obstacle and obtain completely analytic solutions, if the original wave packet is transformed into an eigenstate basis of the field-free Hamiltonian in parabolic coordinates [34,35]:

$$\begin{aligned}\psi_{n,n_1,n_2}(\xi,\eta,\varphi) = N_{n,n_1,n_2} \cdot (\xi\eta)^{\frac{m}{2}} \cdot e^{-\frac{\xi+\eta}{2n}} \\ \times L_{n_1}^m(\xi/n) \cdot L_{n_2}^m(\eta/n) \cdot e^{\imath m\varphi}.\end{aligned} \tag{19}$$

Equation (19) includes two associated Laguerre polynomials $L_{n_i}^m(x)$ [36] that depend on one of the two parabolic coordinates, ξ and η, each. φ is the azimuthal angle. n and m are the principal and magnetic quantum numbers of the eigenstate. Moreover, n_1 and n_2 are parabolic quantum numbers. They obey the relation $n = n_1 + n_2 + m + 1$. N_{n,n_1,n_2} is a normalisation factor:

$$N_{n,n_1,n_2} = \frac{1}{n^{m+2}} \cdot \sqrt{\frac{1}{\pi} \cdot \frac{n_1!}{(m+n_1)!} \cdot \frac{n_2!}{(m+n_2)!}}. \tag{20}$$

Note that the expressions given in [34,35] deviate from equations (19) and (20) due to a different definition of the associated Laguerre polynomials.

The scattering matrix elements that occur in equations (7) and (10) have the general form $\left\langle \psi_f \middle| \hat{\boldsymbol{L}} \middle| \psi_i \right\rangle$. With parabolic eigenstates of the hydrogen atom, the corresponding integrals can be evaluated analytically if the scattering vector $\boldsymbol{q}$ is aligned with the z-axis, meaning $\boldsymbol{q} = q\boldsymbol{e}_z$. The full three-dimensional scattering can be obtained thereafter by rotation of the z-axis around the material system, as will be described later. Hence, the scattering operator that refers to the electron in the hydrogen atom becomes:

$$\hat{\boldsymbol{L}}_z = e^{\imath q \boldsymbol{e}_z \boldsymbol{r}} = e^{\imath q z} = e^{\imath q \frac{\xi-\eta}{2}}. \tag{21}$$

With equations (19) and (21), the scattering matrix element $\langle \psi_f | \hat{L}_z | \psi_i \rangle$ is given as:

$$\begin{aligned}\langle \psi_{n_f,n_{f_1},n_{f_2}} | \hat{L}_z | \psi_{n_i,n_{i_1},n_{i_2}} \rangle &= \frac{1}{4} \cdot N_{n_f,n_{f_1},n_{f_2}} \cdot N_{n_i,n_{i_1},n_{i_2}} \\ \times \int_{\xi=0}^{\infty} \int_{\eta=0}^{\infty} & (\xi+\eta) \cdot e^{-(\xi+\eta)\kappa} \cdot (\xi\eta)^{\frac{m_f+m_i}{2}} \cdot L_{n_{f_1}}^{m_f}(\xi/n_f) \\ & \times L_{n_{f_2}}^{m_f}(\eta/n_f) \cdot L_{n_{i_1}}^{m_i}(\xi/n_i) \cdot L_{n_{i_2}}^{m_i}(\eta/n_i) \\ & \times e^{\imath q \frac{\xi-\eta}{2}} \, d\xi \, d\eta \cdot \int_{\varphi=0}^{2\pi} e^{\imath(m_i-m_f)\varphi} \, d\varphi.\end{aligned} \tag{22}$$

The factor κ in the second line of equation (22) denotes the inverse of the harmonic mean of the principal quantum numbers of the two states, $\kappa = (n_f + n_i)/(2\ n_i\ n_f)$. The last integral over φ does not contain the parabolic coordinates ξ and η. Hence, it can be evaluated independently of the first two integrals. It corresponds to the integral representation of the Kronecker delta δ_{ij} multiplied by a factor of 2π:

$$\int_{\varphi=0}^{2\pi} e^{\imath(m_i-m_f)\varphi} \, d\varphi = 2\pi \ \delta_{m_i,m_f}. \tag{23}$$

The sum $(\xi+\eta)$ in the second line in equation (22) prohibits the separation of the two remaining integrals over ξ and η. However, the sum can be substituted by the negative partial derivative with respect to κ[34], since:

$$(\xi+\eta) \cdot e^{-(\xi+\eta)\kappa} = -\frac{\partial}{\partial \kappa} \, e^{-(\xi+\eta)\kappa}. \tag{24}$$

With equations (23) and (24), equation (22) becomes:

$$\begin{aligned}\langle \psi_{n_f,n_{f_1},n_{f_2}} | \hat{L}_z | \psi_{n_i,n_{i_1},n_{i_2}} \rangle &= -\frac{\pi}{2} \cdot N_{n_f,n_{f_1},n_{f_2}} \cdot N_{n_i,n_{i_1},n_{i_2}} \\ \times \frac{\partial}{\partial \kappa} \Bigg[\int_{\xi=0}^{\infty} & \xi^m \cdot e^{-\xi\left(\kappa - \frac{\imath q}{2}\right)} \cdot L_{n_{f_1}}^m(\xi/n_f) \cdot L_{n_{i_1}}^m(\xi/n_i) \, d\xi \\ & \times \int_{\eta=0}^{\infty} \eta^m \cdot e^{-\eta\left(\kappa + \frac{\imath q}{2}\right)} \cdot L_{n_{f_2}}^m(\eta/n_f) \cdot L_{n_{i_2}}^m(\eta/n_i) \, d\eta \Bigg].\end{aligned} \tag{25}$$

The two remaining integrals in equation (25) are fully separable and can be evaluated independently. Each of these integrals contains a power of the variable of integration, an exponential function, and two associated Laguerre polynomials. A solution for this kind of integral is known from literature[37]:

$$\begin{aligned}&\int_{x=0}^{\infty} x^{\alpha} \cdot e^{-kx} \cdot L_q^{\alpha}(\lambda x) \cdot L_p^{\alpha}(\mu x) \, dx \\ &= \frac{\Gamma(p+q+\alpha+1)}{p!\ q!} \cdot \frac{(k-\lambda)^q \cdot (k-\mu)^p}{k^{(p+q+\alpha+1)}} \\ &\times {}_2F_1\left(-p, -q; -p-q-\alpha; \frac{k \cdot (k-\lambda-\mu)}{(k-\lambda) \cdot (k-\mu)}\right).\end{aligned} \tag{26}$$

The functions on the right-hand side of equation (26) are the Gamma function $\Gamma(n)$ and the Gaussian hypergeometric function ${}_2F_1(a,b;c;z)$. After application of equation (26) to the two integrals in equation (25), the partial derivative with respect to κ can be taken. κ occurs in equation (26) in the second fraction and in the fourth argument of the hypergeometric function. Hence, the derivative of the hypergeometric function with respect to its fourth argument[38] is involved:

$$\frac{\partial}{\partial z} \, {}_2F_1(a,b;c;z) = \frac{ab}{c} \cdot {}_2F_1(a+1,b+1;c+1;z). \tag{27}$$

All other derivatives can be obtained by use of ordinary differentiation rules. Rearrangement of terms and simplification leads to the final expression in equation (28), where $\mathfrak{F}_{\alpha,\beta}(q)$ denotes a product of two hypergeometric functions as defined by equation (29). The indices α and β are either zero or one.

Equations (28) and (29) are a generalisation of the formula that has been published by Schnaidt in 1934[34]. Whereas the latter is limited to a $|\mathbf{1s}\rangle$ ground state, the equations reported here permit the evaluation of any scattering matrix element $\langle \psi_f | \hat{L}_z | \psi_i \rangle$ of the hydrogen atom in the parabolic eigenstate basis.

If a wave packet $|\Psi(t)\rangle$ is defined in terms of real-valued atomic orbitals, a change to the parabolic basis is necessary. Hence, the original basis vectors are expanded in parabolic eigenstates:

$$|\psi_{n,l,|m|=0}\rangle = \sum_{n_1=0}^{n-1} a_{n_1} \cdot |\psi_{n,n_1,n_2}\rangle, \tag{30}$$

$$|\psi_{n,l,|m|\neq 0,\mu}\rangle = \sum_{n_1=0}^{n-|m|-1} \left[a_{n_1} \cdot |\psi_{n,n_1,n_2}\rangle + b_{n_1} \cdot |(\psi_{n,n_1,n_2})^*\rangle \right]. \tag{31}$$

The indices n, l, and m on the left-hand sides of equations (30) and (31) refer to the principal, azimuthal, and magnetic quantum numbers of the atomic orbitals. These orbitals are linear combinations of spherical eigenstates with positive and negative m. Hence, for each value of $|m| \neq 0$ two orbitals exist. In order to distinguish between them, the index μ is introduced. It can either be $+$ or $-$, corresponding to the operation by which the two spherical eigenstates are combined. The degeneracy in $|m|$ is also reflected by the fact that equation (31) contains the parabolic vectors $|\psi_{n,n_1,n_2}\rangle$ as well as their complex conjugates. The multipliers a_{n_1} and b_{n_1} are expansion coefficients. The parabolic quantum number n_2 is unequivocally defined by $n_2 = n - n_1 - |m| - 1$. Expansions for all atomic orbitals with $n \in \{1,2,3,4\}$ are given in the Supplementary Information†.

$$\begin{aligned}
\langle \psi_{n_f,n_{f_1},n_{f_2}} | \hat{L}_z | \psi_{n_i,n_{i_1},n_{i_2}} \rangle &= \frac{4^{m+2}\, n_i^{m+3}\, n_f^{m+3}}{\sqrt{n_{i_1}!\, n_{i_2}!\, n_{f_1}!\, n_{f_2}!}} \cdot \frac{(n_{i_1}+n_{f_1}+m)!}{\sqrt{(n_{i_1}+m)!\ (n_{f_1}+m)!}} \cdot \frac{(n_{i_2}+n_{f_2}+m)!}{\sqrt{(n_{i_2}+m)!\ (n_{f_2}+m)!}} \\
&\times \frac{(n_i - n_f - \imath\, n_i\, n_f\, q)^{n_{i_1}} \cdot (n_f - n_i - \imath\, n_i\, n_f\, q)^{n_{f_1}}}{(n_i + n_f - \imath\, n_i\, n_f\, q)^{n_{i_1}+n_{f_1}+m}} \cdot \frac{(n_i - n_f + \imath\, n_i\, n_f\, q)^{n_{i_2}} \cdot (n_f - n_i + \imath\, n_i\, n_f\, q)^{n_{f_2}}}{(n_i + n_f + \imath\, n_i\, n_f\, q)^{n_{i_2}+n_{f_2}+m}} \\
&\times \frac{1}{(n_i+n_f)^2 + n_i^2\, n_f^2\, q^2} \cdot \frac{1}{(n_i-n_f)^2 + n_i^2\, n_f^2\, q^2} \cdot \left[\frac{n_i\, n_f\, q - \imath \cdot (n_{i_1} - n_{i_2} + n_{f_1} - n_{f_2})}{(n_i+n_f)^2 + n_i^2\, n_f^2\, q^2} \cdot \mathfrak{F}_{0,0}(q) \right. \\
&\left. - \frac{2\,\imath}{(n_i-n_f)^2 + n_i^2\, n_f^2\, q^2} \cdot \frac{n_{i_1}\, n_{f_1}}{n_{i_1}+n_{f_1}+m} \cdot \mathfrak{F}_{1,0}(q) + \frac{2\,\imath}{(n_i-n_f)^2 + n_i^2\, n_f^2\, q^2} \cdot \frac{n_{i_2}\, n_{f_2}}{n_{i_2}+n_{f_2}+m} \cdot \mathfrak{F}_{0,1}(q) \right] \cdot q,
\end{aligned} \tag{28}$$

where

$$\begin{aligned}
\mathfrak{F}_{\alpha,\beta}(q) = {}& {}_2F_1\left(\alpha - n_{i_1},\ \alpha - n_{f_1};\ \alpha - n_{i_1} - n_{f_1} - m;\ 1 + \frac{4\, n_i\, n_f}{(n_i-n_f)^2 + n_i^2\, n_f^2\, q^2} \right) \\
& \times {}_2F_1\left(\beta - n_{i_2},\ \beta - n_{f_2};\ \beta - n_{i_2} - n_{f_2} - m;\ 1 + \frac{4\, n_i\, n_f}{(n_i-n_f)^2 + n_i^2\, n_f^2\, q^2} \right).
\end{aligned} \tag{29}$$

According to the definition of the operator $\hat{L}_z$ in equation (21), the applicability of equations (28) and (29) is hitherto limited to the condition that the $\boldsymbol{q}$-vector is aligned with the z-axis. In order to evaluate the full three-dimensional scattering matrix element $\langle \psi_f | \hat{L} | \psi_i \rangle$, the description has to be extended to any orientation of the $\boldsymbol{q}$-vector. Such an extension is obtainable by use of the rotation matrices $\hat{\mathbf{R}}_y(\theta)$ and $\hat{\mathbf{R}}_z(\phi)$[39]. Their successive action upon a state $|\psi\rangle$ leads to a rotation of the vector around the y- and z-axes of the coordinate system by angles θ and ϕ:

$$|\psi_{\mathbf{R}}(\theta,\phi)\rangle = \hat{\mathbf{R}}_z(\phi)\ \hat{\mathbf{R}}_y(\theta)\ |\psi\rangle. \tag{32}$$

Equation (32) equally describes a rotation of the coordinate system around the fixed state. This is illustrated in figure 1. Since the $\boldsymbol{q}$-vector is aligned with the z-axis, such a rotation alters its orientation with respect to the material system and thus the rotated states $|\psi_{\mathbf{R}}(\theta,\phi)\rangle$ permit an evaluation of the full scattering matrix element with any orientation of the $\boldsymbol{q}$-vector:

$$\langle \psi_f | \hat{L} | \psi_i \rangle = \langle \psi_{f;\mathbf{R}} | \hat{L}_z | \psi_{i;\mathbf{R}} \rangle. \tag{33}$$

If the original state $|\psi\rangle$ is an atomic orbital, the rotated vector $|\psi_{\mathbf{R}}(\theta,\phi)\rangle$ can be expressed as an angle-dependent linear combination of orbitals that share the same n and l. This can be ascribed to the fact that the magnetic quantum number m defines the orientation of the angular momentum.

$$\begin{aligned}
|\psi_{n,l,|m|,\mu;\mathbf{R}}(\theta,\phi)\rangle = {}& r_0(\theta,\phi) \cdot |\psi_{n,l,m_{\mathbf{R}}=0}\rangle \\
& + \sum_{m_{\mathbf{R}}=1}^{l} \sum_{\mu_{\mathbf{R}}=+}^{-} r_{m_{\mathbf{R}},\mu_{\mathbf{R}}}(\theta,\phi) \cdot |\psi_{n,l,m_{\mathbf{R}},\mu_{\mathbf{R}}}\rangle.
\end{aligned} \tag{34}$$

The angle-dependent expansion coefficients $r_0(\theta,\phi)$ and $r_{m_{\mathbf{R}},\mu_{\mathbf{R}}}(\theta,\phi)$ in equation (34) can be determined by use of $\hat{\mathbf{R}}_y(\theta)$ and $\hat{\mathbf{R}}_z(\phi)$. For that the atomic orbital $|\psi_{n,l,|m|,\mu}\rangle$ is written in Cartesian coordinates. The rotation matrices transform these coordinates into a weighted sum of products $\prod_i^l \alpha_i$ with $\alpha_i \in \{x,y,z\}$. These products are substituted with their corresponding linear

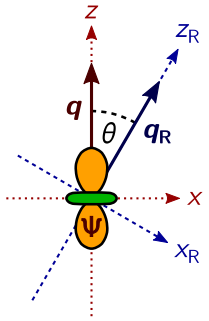

Fig. 1 Rotation of the $\boldsymbol{q}$-vector around the material system Ψ by an angle θ. Since the $\boldsymbol{q}$-vector is, by definition of $\hat{L}_z$, aligned with the z-axis, its rotation is described by a rotation of the coordinate system. The original coordinates x and z are transformed into x_{R} and z_{R}. Thereby, $\boldsymbol{q}$ becomes $\boldsymbol{q}_{\mathbf{R}}$.

combinations of atomic orbitals. A rearrangement of terms finally yields the coefficients. A more detailed description as well as expansions for rotations of all $|\mathbf{d}\rangle$ and $|\mathbf{f}\rangle$ orbitals are given in the Supplementary Information†.

The atomic orbitals in both terms on the right-hand side of equation (34) can, in turn, be expanded in the parabolic eigenstate basis, as it was previously shown in equations (30) and (31). The angles θ and ϕ refer to the orientation of the $\boldsymbol{q}$-vector and are not affected by the integration over the real space coordinates ξ, η, and φ in equation (22). Hence, a full three-dimensional scattering matrix element defined in a real-valued atomic orbital basis can be expanded in terms of the one-dimensional elements given in equations (28) and (29):

$$\begin{aligned}\langle \psi_{n_f,l_f,|m_f|,\mu_f} | \hat{\boldsymbol{L}} | \psi_{n_i,l_i,|m_i|,\mu_i} \rangle = \sum_{m_{\mathbf{R}}} \sum_{n_{f_1}} \sum_{n_{i_1}} t_{m_{\mathbf{R}},n_{f_1},n_{i_1}}(\theta,\phi) \\ \times \langle \psi_{n_f,n_{f_1},n_{f_2}} | \hat{L}_z | \psi_{n_i,n_{i_1},n_{i_2}} \rangle,\end{aligned} \tag{35}$$

where the Kronecker delta in equation (23) led to a reduction of the two sums over $m_{f,\mathbf{R}}$ and $m_{i,\mathbf{R}}$ to a single one over $m_{\mathbf{R}}$. Its lower and upper limits are zero and $\min(l_f,l_i)$. The sums over n_{f_1} and n_{i_1} run from zero to $n_f - m_{\mathbf{R}} - 1$ and $n_i - m_{\mathbf{R}} - 1$, respectively. The expansion coefficients $t_{m_{\mathbf{R}},n_{f_1},n_{i_1}}(\theta,\phi)$ can be derived from the coefficients in equations (30), (31), and (34). No complex conjugate vector $|(\psi_{n,n_1,n_2})^*\rangle$ enters the matrix elements explicitly, since for parabolic eigenstates:

$$\langle \psi_f | \hat{L}_z | \psi_i \rangle = \langle \psi_f^* | \hat{L}_z | \psi_i^* \rangle, \tag{36}$$

$$\langle \psi_f | \hat{L}_z | \psi_i^* \rangle = \langle \psi_f^* | \hat{L}_z | \psi_i \rangle = 0. \tag{37}$$

Equations (36) and (37) can be deduced from equations (19) and (22): A parabolic eigenstate is complex only in the exponential $e^{\imath m\varphi}$. Taking the conjugates of both, the bra and the ket, leads to a change of sign of the exponent in equation (23). This change does not alter the result of the integration. If, in contrast, only one vector is complex conjugate, the difference $m_i - m_f$ in equation (23) is transformed into the sum $m_i + m_f$. Since m_i and m_f are positive integers, the integral has to vanish.

5 Illustrations

In the following, the results of sections 2 and 4 are applied to an electronic wave packet of superposed and equally weighted $|\mathbf{3d}_{z^2}\rangle$ and $|\mathbf{4f}_{z^3}\rangle$ orbitals of the hydrogen atom. Time-resolved X-ray scattering patterns of this wave packet have already been calculated numerically by Dixit *et al.* [18]. The compact density operator formalism the authors have used to demonstrate the difference between the quantized and the semi-classical descriptions of the scattering, however, makes a more detailed analysis of the nature of the patterns difficult. Here, the elements D_i and O_{ij} are evaluated separately, allowing not only a more efficient computation but also a more illustrative discussion of the time-dependence of the X-ray scattering signal.

By use of atomic units and equation (1), the non-stationary electronic wave packet is defined as:

$$|\Psi(t)\rangle = \frac{1}{\sqrt{2}} \cdot \left(e^{-\imath E_3 t/\hbar} \cdot |\mathbf{3d}_{z^2}\rangle + e^{-\imath E_4 t/\hbar} \cdot |\mathbf{4f}_{z^3}\rangle \right). \tag{38}$$

The energies in equation (38) are $E_3 = -1/18$ a.u. ≈ -1.51 eV and $E_4 = -1/32$ a.u. ≈ -0.85 eV. With equations (6) and (12), the scattering signal of this wave packet is described by:

$$\begin{aligned}\frac{dS}{d\Omega} \propto D_3 + D_4 + 2\, e^{-\frac{1}{2}(\omega\sigma)^2} \cdot \Big(\cos(\omega\tau) \\ \times \mathrm{Re}\big[O_{3,4}\big] + \sin(\omega\tau)\ \mathrm{Im}\big[O_{3,4}\big] \Big).\end{aligned} \tag{39}$$

The indices 3 and 4 in equation (39) and in the following refer to the $|\mathbf{3d}_{z^2}\rangle$ and $|\mathbf{4f}_{z^3}\rangle$ orbitals, respectively. The angular frequency of the wave packets is $\omega = 7/288$ a.u. ≈ 1.0/fs.

According to equations (7) and (10), the elements in equation (39) are given as:

$$D_3 = \frac{1}{2} \cdot \sum_f^{\infty} \left| \tilde{\boldsymbol{L}}_{f,3} \right|^2 W_{f,3,3}(\Delta\omega), \tag{40}$$

$$D_4 = \frac{1}{2} \cdot \sum_f^{\infty} \left| \tilde{\boldsymbol{L}}_{f,4} \right|^2 W_{f,4,4}(\Delta\omega), \tag{41}$$

$$O_{3,4} = \frac{1}{2} \cdot \sum_f^{\infty} \tilde{\boldsymbol{L}}_{f,3}\, \tilde{\boldsymbol{L}}_{f,4}^*\, W_{f,3,4}(\Delta\omega). \tag{42}$$

The off-diagonal element in equation (42) contains the same matrix elements as equations (40) and (41). These matrix elements have to be evaluated once and then all three elements, D_3, D_4, and $O_{3,4}$, can be formed as their corresponding products. Following the previous section, exact solutions to the matrix elements are obtainable by expansion in the parabolic eigenstate basis. Note that only the states involved in the wave packet, but not the vectors $|\psi_f\rangle$ have to be rotated by equations (32) and (34). The sum over f includes all states degenerate in m once and is therefore unaffected by rotation. Further details of the evaluation are given in the Supplementary Information†.

Here, the sum over f in equations (40) to (42) has been truncated at the principal quantum number $n_f = 50$. The values of D_3, D_4, and 2 $\mathrm{Im}\big[O_{3,4}\big]$ at the converged $\boldsymbol{q}$-space coordinates of the maximum of $\mathrm{Im}\big[O_{3,4}\big]$ at different values of truncation n_f are shown in figure 2. Following Dixit *et al.* [18], it is assumed that the incident X-ray probe pulse propagates along the y-axis and has a mean photon energy of $\langle E_0 \rangle = 4$ keV and a time duration (FWHM) of $d_\mathrm{p} = 1$ fs. All scattered photons within the range of $\pm\Delta\omega = 0.25$ eV around $\langle E_0 \rangle$ are detected. It becomes apparent that in all three cases electronic states with principal quantum numbers above $n_f \approx 20$ contribute only negligibly to the total value. Physically, every matrix element that involves a vector $|\psi_f\rangle$ with $n_f \notin \{3,4\}$ corresponds to an electronic Raman transition induced by inelastic scattering of a photon. Thus, the convergence of the values in figure 2 can be related to the fact that transitions to electronic states in the proximity of those already occupied in the wave packet are the most probable to contribute

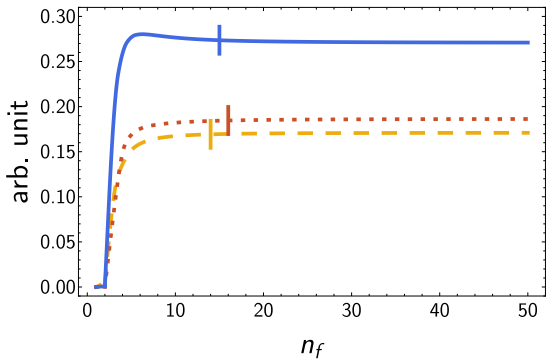

Fig. 2 Values of the elements D_3 (- - -), D_4 (· · ·), and $2\,\mathrm{Im}[O_{3,4}]$ (——) with increasing number of states $|\psi_f\rangle$. The variable n_f denotes the principal quantum number at which the sum over f is truncated. The incident probe pulse propagates along the y-axis and has a mean photon energy of $\langle E_0\rangle = 4$ keV and a time duration (FWHM) of $d_\mathrm{p} = 1$ fs. All scattered photons within the range of $\pm\Delta\omega = 0.25$ eV around $\langle E_0\rangle$ are detected. The elements have been evaluated at $q \approx 0.45/\text{Å}$, $\theta_q \approx 84°$, and $\phi_q = 90°$, *i.e.* the point in the q_x-q_z plane at which $\mathrm{Im}[O_{3,4}]$ has its maximum. The vertical lines mark the points where the elements are converged to less than 1% deviation of their values at $n_f = 50$. These points are $n_f = 14$, $n_f = 16$, and $n_f = 15$.

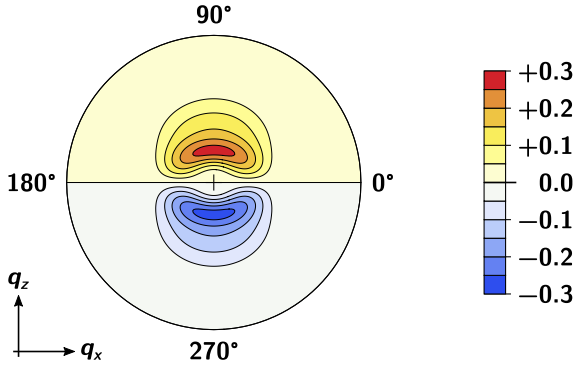

Fig. 3 Contour plot of two times the imaginary part of the element $O_{3,4}$ in the q_x-q_z plane. $O_{3,4}$ represents spatial coherences in the X-ray scattering signal of superposed and equally weighted $|\mathbf{3d}_{z^2}\rangle$ and $|\mathbf{4f}_{z^3}\rangle$ orbitals of the hydrogen atom. The incident probe pulse propagates along the y-axis and has a mean photon energy of $\langle E_0\rangle = 4$ keV and a time duration (FWHM) of $d_\mathrm{p} = 1$ fs. All scattered photons within the range of $\pm\Delta\omega = 0.25$ eV around $\langle E_0\rangle$ are detected. With photons scattered up to 60° and $q_\mathrm{max} \approx 2.03/\text{Å}$, the q_x and q_z coordinates take values in between $\pm 1.66/\text{Å}$. The angular coordinate is the azimuthal angle of the $\boldsymbol{q}$-vector, ϕ_q. The approximation $\omega_\mathrm{s} \approx \omega_0$ has been applied.

to the detected scattering signal. The convergence in figure 2 also illustrates that it is not generally sufficient to approximate the elements D_i by their elastic contributions. At the considered $\boldsymbol{q}$-space coordinate, inelastic scattering accounts for more than 44% of D_3 and 64% of D_4. This becomes even more dramatic at larger values of q, where inelastic scattering is usually stronger than elastic.

Further evaluation of $O_{3,4}$ reveals that its real part vanishes. Equation (39) therefore reduces to:

$$\frac{dS}{d\Omega} \propto D_3 + D_4 + 2\, e^{-\frac{1}{2}(\omega\sigma)^2} \sin(\omega\tau)\, \mathrm{Im}[O_{3,4}]. \qquad (43)$$

According to equation (43), the differential scattering signal experiences a sinusoidal modulation with pump-probe delay τ over a period of $T = 576\pi/7$ a.u. ≈ 6.253 fs. The global magnitude of this modulation is limited by the probe pulse duration $d_\mathrm{p} = 2\sqrt{2\ln 2}\,\sigma$, whereas its spatial pattern is described solely by the imaginary part of $O_{3,4}$.

A contour plot of $2\,\mathrm{Im}[O_{3,4}]$ is shown in figure 3. The scattering pattern lies in the q_x-q_z plane and photons scattered at angles of at most 60° are detected. With the approximation $\omega_\mathrm{s} \approx \omega_0$, the norm of the $\boldsymbol{q}$-vector takes maximum values of $q_\mathrm{max} \approx 2.03/\text{Å}$. The pattern in figure 3 displays a dihedral D_1 rosette group symmetry that involves a single reflection through the q_z-axis. Its values are positive at $q_z > 0$ (or $\phi_q < 180°$), but negative when $q_z < 0$ (or $\phi_q > 180°$). As a consequence, the imaginary part of $O_{3,4}$ causes the differential scattering signal to oscillate along the q_z-axis and breaks any higher symmetry that D_3 and D_4 may have. The pattern is not centrosymmetric and cannot be related to absolute squares of Fourier transformed, real-valued functions, as it has been discussed in section 3.

After evaluation of the remaining elements, $D_3 + D_4$, the full scattering signal of the wave packet is obtained. In figure 4, scattering patterns computed for five different pump-probe delays τ are shown: at zero, one-fourth, one-half, three-fourth, and one times the period of the oscillation T. They match the patterns published by Dixit *et al.*[18]. With $d_\mathrm{p} = 2\sqrt{2\ln 2}\,\sigma = 1.0$ fs, the exponential in equation (43) constrains the magnitude by which the element $O_{3,4}$ can contribute to at most 91%. Since the time-dependent term in equation (43) involves a sine function, scattering patterns at zero, one-half, and one times T are described exclusively by the time-independent average $D_3 + D_4$. They display a centrosymmetric D_2 rosette group symmetry that contains a two-fold rotation and reflections through both the q_x- and the q_z-axis. The patterns can correspond to the static average one would measure without any time-resolution. The higher D_2 symmetry of the patterns is broken to D_1, as soon as the contributions of $O_{3,4}$ are non-zero. In between zero and one-fourth times T, the scattering signal is shifted into the upper semi circle of the pattern to azimuthal angles of $\phi_q < 180°$. At one-fourth of T, most of the intensity is observed at $q_z > 0$. After this, the signal moves downwards in direction of the lower semi circle of the pattern to azimuthal angles of $\phi_q > 180°$, until the intensity at $q_z < 0$ reaches its maximum at three-fourth of T. Finally, the signal is shifted upwards again, closing the cycle at T.

Hence, the scattering patterns in figure 4 show temporal variations that have already been deduced from figure 3 alone. This illustrates that the elements O_{ij} are of prime importance for the simulation and understanding of the time-resolved differential X-ray scattering signal of non-stationary electronic wave packets.

Finally, the effect of the pulse duration d_p and the range of detected frequencies $\Delta\omega$ upon the scattering signal will be illustrated. Figure 5**A** shows the total scattering signal at different pump-probe delays τ for one point in $\boldsymbol{q}$-space and three probe pulse durations d_p. The intensity of the signal decreases with d_p. As discussed in section 2, less photons are detected at shorter pulse durations. In figure 5**B**, only the modulation, *i.e.* the total signal from **A** minus its time-independent average, is shown. The

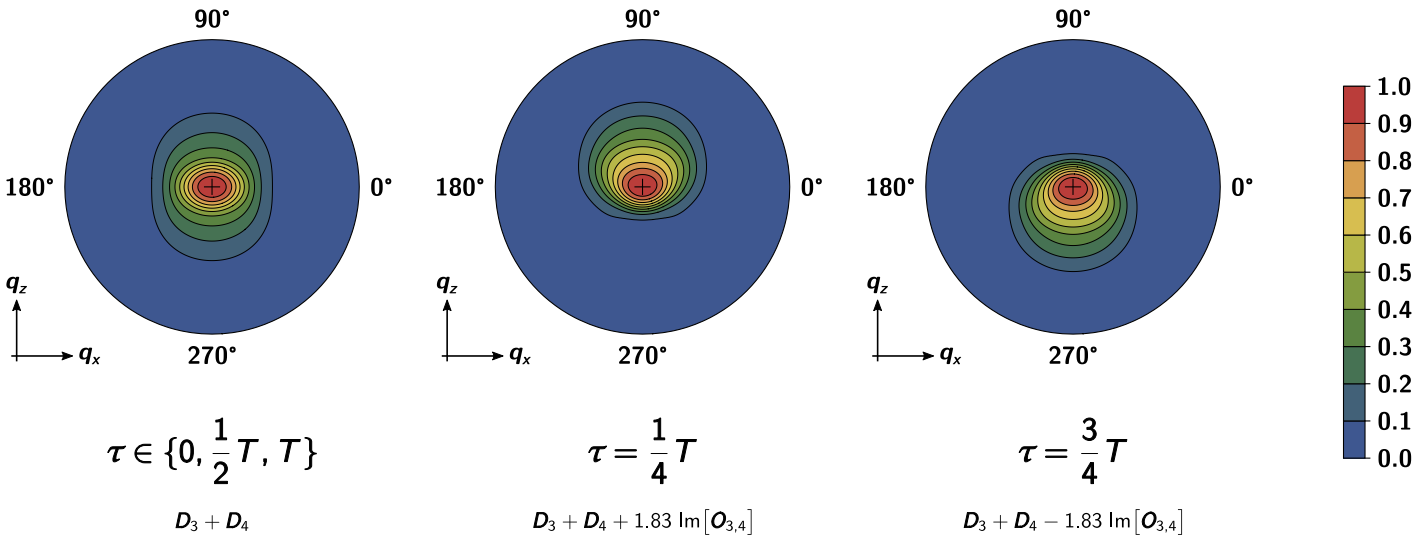

Fig. 4 Contour plots of X-ray scattering patterns in the q_x-q_z plane at different points in time. The radiation is scattered by a non-stationary wave packet of superposed and equally weighted $|\mathbf{3d}_{z^2}\rangle$ and $|\mathbf{4f}_{z^3}\rangle$ orbitals of the hydrogen atom. The incident probe pulse propagates along the y-axis and has a mean photon energy of $\langle E_0 \rangle = 4$ keV and a time duration (FWHM) of $d_\mathrm{p} = 1$ fs. All scattered photons within the range of $\pm\Delta\omega = 0.25$ eV around $\langle E_0 \rangle$ are detected. With photons scattered up to 60° and $q_\mathrm{max} \approx 2.03/\text{Å}$, the q_x and q_z coordinates take values in between $\pm 1.66/\text{Å}$. The angular coordinate is the azimuthal angle of the $\boldsymbol{q}$-vector, ϕ_q. The time τ is the pump-probe delay and given in units of the oscillation period of the wave packet, $T \approx 6.253$ fs. The scattering patterns have been convoluted with a Gaussian shaped intensity time profile of the incident probe pulse. The approximation $\omega_\mathrm{s} \approx \omega_0$ has been applied. It is shown how the elements D_3, D_4, and $O_{3,4}$ defined in equations (40) to (42) add up to the patterns.

modulation has a larger amplitude for a pulse duration of 1.0 fs than for 0.1 fs and 4.0 fs. Hence, the amplitude of the modulation has to display an optimum at a pulse duration in the vicinity of 1.0 fs, as also observed previously[18].

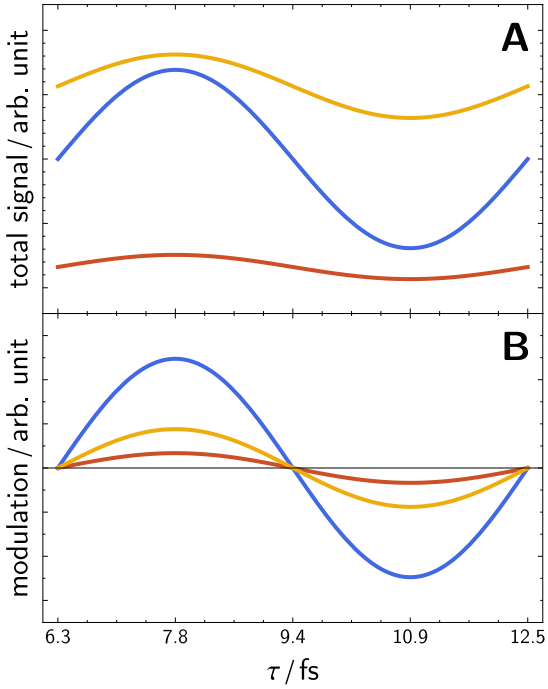

Fig. 5 A: Total scattering signal and **B**: its time-dependent modulation at different pump-probe delays τ for probe pulse durations d_p of 4.0 fs (—), 1.0 fs (—), and 0.1 fs (—). **A** and **B**: The signals have been evaluated at $q \approx 0.45/\text{Å}$, $\theta_q \approx 84°$, and $\phi_q = 90°$ with a range of detection of $\pm\Delta\omega = 0.25$ eV around $\langle E_0 \rangle = 4$ keV.

This becomes even more apparent in figure 6**A**: The time-independent average $D_3 + D_4$ approaches zero as $d_\mathrm{p} \to 0$ and a finite limit as $d_\mathrm{p} \to \infty$. The amplitude of the time-dependent modulation $2\exp(-\frac{1}{2}(\omega\sigma)^2)\ \mathrm{Im}[O_{3,4}]$ becomes zero in both cases and has an optimum in between at $d_\mathrm{p} \approx 1.63$ fs. The amplitude of the relative modulation, defined as the ratio of the absolute amplitude and the average, is displayed in figure 6**A** as well. It approaches a finite value as $d_\mathrm{p} \to 0$ and zero as $d_\mathrm{p} \to \infty$. Moreover, it displays an optimum at $d_\mathrm{p} \approx 1.31$ fs. The ratio of detected photons that carry time-dependent information to those that do not is the largest here. This confirms the previously observed, somewhat counterintuitive behaviour that time-dependent scattering signal loses contrast (amplitude of the modulation) at very short probe pulse durations[18]. It can be seen, however, that the scattering signal does not become completely time-independent as $d_\mathrm{p} \to 0$. Even though the amplitude of the absolute modulation vanishes and the signal may eventually become too weak to be detected, the proportion by which the modulation contributes to the total signal approaches a constant.

Following the general discussion of section 2, the existence of the optimum in the amplitude of the modulation can be ascribed to the weights $W_{fij}(\Delta\omega)$. The loss of scattering signal and contrast at very short pulse durations is a direct consequence of the limited range of detection $\Delta\omega$. As shown in figure S3 of the Supplementary Information†, not only the modulation but also the inelastic part of the static average displays an optimum. This is expected from the investigation in section 2. Furthermore, the position of the optimum depends on the value of $\Delta\omega$. Figure 6**B** reveals that the optimum of the amplitude is shifted towards shorter pulse durations when $\Delta\omega$ is increased and more photons can be detected.

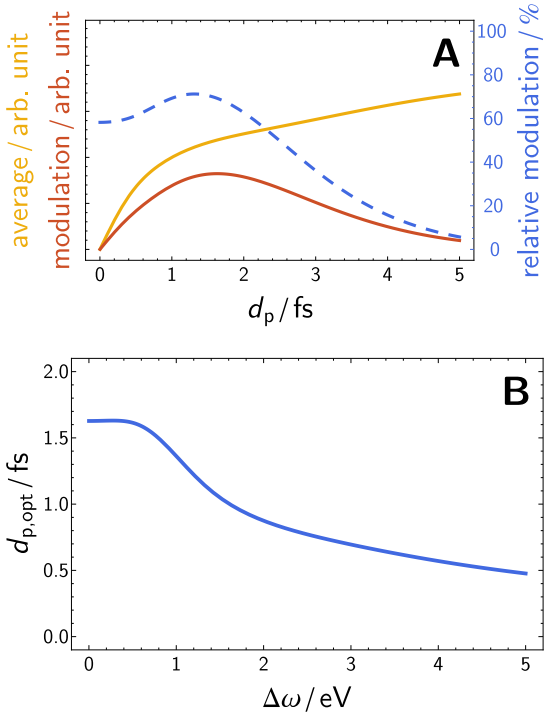

Fig. 6 A: Average (——), amplitude of the modulation (——), and amplitude of the relative modulation (- - -) of the scattering signal at different probe pulse durations d_p. A range of detection of $\pm\Delta\omega = 0.25$ eV around $\langle E_0 \rangle = 4$ keV has been chosen. **B**: Pulse duration $d_{p,opt}$ at which the amplitude of the modulation displays its optimum for different ranges of detection $\pm\Delta\omega$ around $\langle E_0 \rangle = 4$ keV. **A** and **B**: The signals have been evaluated at $q \approx 0.45/\text{Å}$, $\theta_q \approx 84°$, and $\phi_q = 90°$.

6 Summary and Conclusions

The time-resolved X-ray scattering signal of non-stationary electronic wave packets in atomic systems is described in detail and different contributions are identified as the elements D_i and O_{ij}. They refer to the static and non-stationary scattering contributions, respectively. Whereas the former corresponds to absolute squares of Fourier transformed expectation values of the one-electron density operator, the latter represents spatial correlations of the X-ray photon and different states of the material system. The time-dependent part of the scattering signal solely comprises these correlations. For a probe pulse with a Gaussian intensity time profile, it is shown that neither the pump-probe delay nor the properties of the pulse enter the matrix elements directly. They are arguments of a function that multiplicatively weights the contribution of O_{ij}. This enables cost-efficient simulations for different points in time under various experimental conditions.

Moreover, it is demonstrated how to express the X-ray scattering signal of non-stationary electronic wave packets in the hydrogen atom analytically. By rotation of the wave packet in the parabolic eigenstate basis, the scattering matrix elements can be evaluated exactly without numerical integration. This approach is, in principle, also applicable to atomic systems with single non-stationary Rydberg electrons that are decoupled from the remaining stationary core electrons, as a numerical investigation of scattering by the helium atom[27] suggests. Distinctive features of time-resolved X-ray scattering by non-stationary electronic wave packets are illustrated by reference to the wave packet that has been introduced by Dixit *et al.*[18]. It is shown that the elements O_{ij} are characteristic of time-resolved scattering and determine the symmetry the patterns display. Finally, it has been demonstrated that the loss of contrast of the time-dependent scattering signal at very short probe pulse durations is merely a consequence of the energy resolution of the detector.

A further extension of the analysis presented here could involve a detailed investigation of time-resolved X-ray scattering by diatomic molecules in non-stationary nuclear and electronic states. This may eventually support prospective X-ray scattering experiments that address the electronic time-scale in chemistry[40–42].

Acknowledgments

Mats Simmermacher thanks Dietrich Krebs for prolific discussions that, among other things, have led to the usage of the parabolic eigenstate basis.

References

1 P. Emma *et al.*, *Nat. Photon.*, 2010, **4**, 641–647.
2 T. Ishikawa *et al.*, *Nat. Photon.*, 2012, **6**, 540–544.
3 European XFEL, `http://www.xfel.eu`, Accessed on: May 18, 2017.
4 SwissFEL, `http://www.psi.ch/swissfel`, Accessed on: May 18, 2017.
5 D. Arnlund *et al.*, *Nat. Methods*, 2014, **11**, 923–926.
6 K. H. Kim *et al.*, *Nature*, 2015, **518**, 385–389.
7 M. Levantino, G. Schirò, H. T. Lemke, C. Grazia, J. M. Glownia, Z. Diling, M. Chollet, H. Ihee and A. C. amd M. Cammarata, *Nat. Commun.*, 2015, **6**, 6772.
8 J. G. Kim, T. W. Kim, J. Kim and H. Ihee, *Accounts Chem. Res.*, 2015, **48**, 2200–2208.
9 M. Minitti *et al.*, *Phys. Rev. Lett.*, 2015, **114**, 255501.
10 J. M. Budarz, M. P. Minitti, D. V. Cofer-Shabica, B. Stankus, A. Kirrander, J. B. Hastings and P. M. Weber, *J. Phys. B*, 2016, **49**, 034001.
11 K. Haldrup *et al.*, *J. Phys. Chem. B*, 2016, **120**, 1158–1168.
12 E. Biasin *et al.*, *Phys. Rev. Lett.*, 2016, **117**, 013002.
13 A. A. Zholents and W. M. Fawley, *Phys. Rev. Lett.*, 2004, **92**, 224801.
14 E. L. Saldin, E. A. Schneidmiller and M. V. Yurkov, *Phys. Rev. Accel. Beams*, 2006, **9**, 050702.
15 T. Tanaka, *Phys. Rev. Lett.*, 2013, **110**, 084801.
16 D. J. Dunning, B. W. J. McNeil and N. R. Thompson, *Phys. Rev. Lett.*, 2013, **110**, 104801.
17 E. Prat and S. Reiche, *Phys. Rev. Lett.*, 2015, **114**, 244801.
18 G. Dixit, O. Vendrell and R. Santra, *Proc. Natl. Acad. Sci. U.S.A.*, 2012, **109**, 11636–11640.
19 P. A. M. Dirac, *Proc. R. Soc. Lond. A*, 1927, **114**, 243–265.
20 M. Ben-Nun, T. J. Martínez, P. M. Weber and K. R. Wilson, *Chem. Phys. Lett.*, 1996, **262**, 405–414.
21 M. Ben-Nun, J. Cao and K. R. Wilson, *J. Phys. Chem. A*, 1997, **101**, 8743–8761.

22 J. Cao and K. R. Wilson, *J. Phys. Chem. A*, 1998, **102**, 9523–9530.
23 S. Bratos, F. Mirloup, R. Vuilleumier and M. Wulff, *J. Chem. Phys.*, 2002, **116**, 10615–10625.
24 N. E. Henriksen and K. B. Møller, *J. Phys. Chem. B*, 2008, **112**, 558–567.
25 U. Lorenz, K. B. Møller and N. E. Henriksen, *Phys. Rev. A*, 2010, **81**, 023422.
26 K. B. Møller and N. E. Henriksen, *Struct. Bond.*, 2012, **142**, 185–212.
27 G. Dixit and R. Santra, *J. Chem. Phys.*, 2013, **138**, 134311.
28 G. Dixit, J. M. Slowik and R. Santra, *Phys. Rev. A*, 2014, **89**, 043409.
29 H. Suominen and A. Kirrander, *Phys. Rev. Lett.*, 2014, **112**, 043002.
30 A. Kirrander, K. Saita and D. V. Shalashilin, *J. Chem. Theory Comput.*, 2016, **12**, 957–967.
31 I. Waller and D. R. Hartree, *P. R. Soc. Lond. A*, 1929, **124**, 119–142.
32 G. Friedel, *C. R. Hebd. Acad. Sci.*, 1913, **157**, 1533–1536.
33 D. A. Varshalovich, A. N. Moskalev and V. K. Khersonskii, *Quantum Theory of Angular Momentum*, World Scientific, 1988, p. 148.
34 F. Schnaidt, *Annalen der Physik*, 1934, **413**, 89–112.
35 H. A. Bethe and E. E. Salpeter, *Quantum Mechanics of One- and Two-Electron Atoms*, Springer, 1957, p. 29.
36 M. Abramowitz and I. A. Stegun, *Handbook of Mathematical Functions*, Dover Publications, 1964, p. 778.
37 A. Erdélyi, W. Magnus, F. Oberhettinger and F. G. Tricomi, *Tables of Integral Transforms Vol. I*, McGraw-Hill, 1954, p. 175.
38 W. Magnus and F. Oberhettinger, *Formeln und Sätze für die Speziellen Funktionen der Mathematischen Physik*, Springer, 1948, p. 11.
39 G. B. Arfken and H. J. Weber, *Mathematical Methods for Physicists*, Academic Press, 2005, p. 203.
40 M. Grønager and N. E. Henriksen, *Chem. Phys. Lett.*, 1997, **278**, 166–174.
41 L. S. Cederbaum and J. Zobeley, *Chem. Phys. Lett.*, 1999, **307**, 205–210.
42 F. Remacle and R. D. Levine, *Proc. Natl. Acad. Sci. U.S.A.*, 2006, **103**, 6793–6798.